Observation of ionization enhancement in two-color circularly polarized laser fields

doi: 10.1103/PhysRevA.96.023402

Observation of ionization enhancement in two-color circularly polarized laser fields

Christopher A. Mancuso,[1] Kevin M. Dorney,[1] Daniel D. Hickstein,[1] Jan L. Chaloupka,[2] Xiao-Min Tong,[3] Jennifer L. Ellis,[1] Henry C. Kapteyn,[1] and Margaret M. Murnane[1]

[1]*JILA, Department of Physics, University of Colorado Boulder and NIST, Boulder, Colorado 80309, USA*

[2]*Department of Physics and Astronomy, University of Northern Colorado, Greeley, Colorado 80639, USA*

[3]*Center for Computational Sciences and Graduate School of Pure and Applied Science, University of Tsukuba, Tsukuba, Ibaraki 305-8571, Japan*

(Received 6 January 2017; published 2 August 2017)

When atoms are irradiated by two-color circularly polarized laser fields the resulting strong-field processes are dramatically different than when the same atoms are irradiated by a single-color ultrafast laser. For example, electrons can be driven in complex two-dimensional trajectories before rescattering or circularly polarized high harmonics can be generated, which was once thought impossible. Here, we show that two-color circularly polarized lasers also enable control over the ionization process itself and make a surprising finding: the ionization rate can be enhanced by up to 700% simply by switching the relative helicity of the two-color circularly polarized laser field. This enhancement is experimentally observed in helium, argon, and krypton over a wide range of intensity ratios of the two-color field. We use a combination of advanced quantum and fully classical calculations to explain this ionization enhancement as resulting in part due to the increased density of excited states available for resonance-enhanced ionization in counter-rotating fields compared with co-rotating fields. In the future, this effect could be used to probe the excited state manifold of complex molecules.

DOI: 10.1103/PhysRevA.96.023402

I. INTRODUCTION

When a strong laser field ($\sim 10^{13}\,\mathrm{W\,cm^{-2}}$) interacts with an atom or molecule, an electron can be liberated from the ion, accelerated by the laser field, and then driven back to the parent ion [1–4]. This free electron can then interact a second time with the ion in a variety of ways, including radiatively recombining via high-harmonic generation (HHG) [1,5,6] or rescattering from the ion core. In the simplest semiclassical picture of HHG, the electron can return to the parent ion with high kinetic energy and then any excess energy greater than the ionization potential can then be emitted as a high-harmonic photon. When the HHG process is properly phase matched, a bright coherent beam of extreme ultraviolet (EUV) or soft-x-ray light is generated [6–10], which can be used to uncover coupled dynamics in materials with femtosecond-to-attosecond temporal resolution [11–15], and can also be used for high-resolution imaging [16–19]. Alternatively, if the electron does not recombine upon reencountering the ion, it may rescatter from the ion, encoding information about the subangstrom and subfemtosecond structure of the scattering potential into the photoelectron momentum distribution [20–22].

Recently, the unusual optical wave forms generated through the mixing of two circularly polarized fields at different wavelengths (which we refer to here as a *bicircular field*) have enabled exciting new capabilities in both HHG and strong-field ionization (SFI). In the case of HHG, the use of a bicircular driving laser field provides a bright (i.e., phase matched) source of *circularly polarized* EUV [23–29] and soft-x-ray [30] beams with sufficient flux for applications in magnetic spectroscopies of materials [28,30]. In the case of SFI, bicircular fields allow electrons to be driven in two-dimensional trajectories prior to rescattering from the parent ion [31–38]. Interestingly, the shape of the bicircular wave form—and therefore the physics of the HHG and SFI processes—can be modified by changing the relative wavelengths, intensities, and ellipticities of the two driving fields [29–31,36]. Recent studies have explored the acceleration step as well as the rescattering or recombination steps of SFI and HHG driven by a bicircular field [30,36,39–41].

However, to date little attention has been devoted to the ionization step [37] in strong bicircular fields, despite the fact that helicity-induced changes to this first step could have a profound impact on the subsequent physics of rescattering or recombination. Past studies have investigated the dependence of the ionization rate on the relative helicity of a one-color circularly polarized field and the atomic orbital from which the electron is ionized, showing that at low (high) intensities, a co(counter)-rotating geometry is preferred [42–46]. Additionally, recent work has looked at helicity-dependent ionization with a few vacuum ultraviolet and near-infrared (NIR) photons [47–51], in which the probability of ionization via different resonant pathways in He^+ was determined, and a helicity-dependent ac Stark shift was observed [51].

In this article, we present the observation of an intensity-dependent ionization enhancement of helium, argon, and krypton atoms, where many photons from each driving laser field contribute significantly to the ionization process. We show that at intermediate intensities, there is an enhancement in the ionization yield for counter-rotating bicircular fields. For low laser intensities, ionization is perturbative and strongly influenced by the second-harmonic field. For high intensities, adiabatic tunnel ionization dominates. Moreover, in both the low and high intensity regimes, the ionization rates are similar from co- and counter-rotating fields, as expected. However, at intermediate laser intensities, the observed ionization rate differs significantly from both the adiabatic tunneling and perturbative limits. Here, by switching the relative helicity of the fields with respect to one another (i.e., counter-rotating versus co-rotating), we can precisely preserve the peak field strength, as well as the integrated electric field, while changing only the shape and spin-angular momenta of the field [Fig. 1(a)]. This technique allows us to observe a strong enhancement

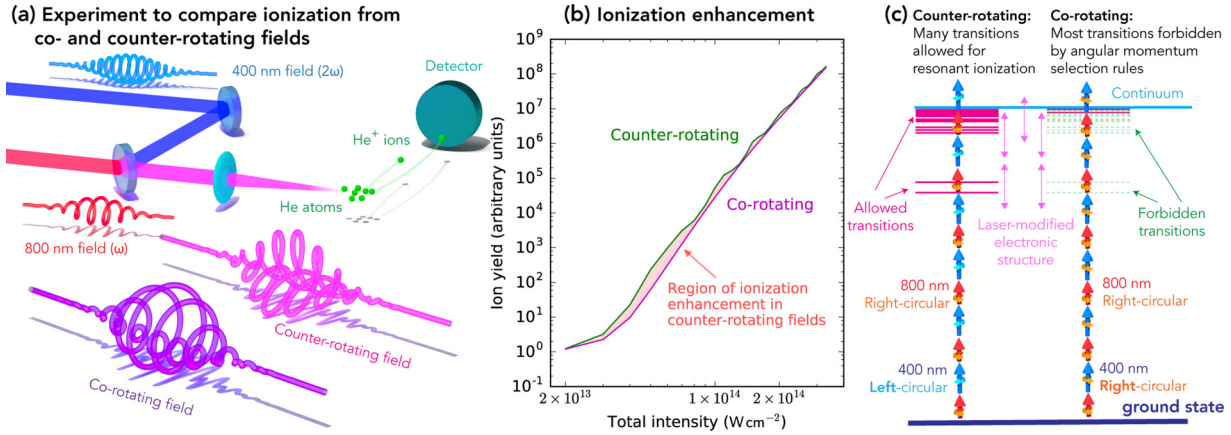

FIG. 1. (a) Experimental scheme used to study ionization rates in two-color (ω,2ω) circularly polarized fields consisting of a femtosecond laser system, a Mach-Zehnder interferometer, and a time-of-flight spectrometer. (b) He^+ yields from TDSE simulations show a significant enhancement in ionization for counter-rotating fields at intermediate intensities. (c) In the presence of a strong-field laser, the energy levels are dynamically broadened and shifted [60]. In counter-rotating fields, the mixture of $+1$ and -1 spins results in a field with near-zero angular momentum, allowing enhanced ionization via many resonant states. In co-rotating fields, the photons have either all $+1$ spin or -1 spin, thus only excited states of high angular momentum can serve as resonant states.

of the ionization rate (up to 700%) in counter-rotating fields compared to co-rotating fields [Fig. 1(b)]. Our experimental findings are confirmed using numerical simulations of the time-dependent Schrödinger equation (TDSE) [52,53], which contain the entire manifold of quantum states. Additionally, the TDSE simulations allow us to propose a possible mechanism behind the observed ionization enhancement in the quantum picture; counter-rotating fields can access many ionization pathways that progress through highly excited states with a low total angular momentum quantum number. In contrast, for co-rotating fields, most of these intermediate states are forbidden by spin-angular momentum selection rules [Fig. 1(c)]. Interestingly, we observe a similar ionization enhancement in fully classical simulations using the classical ensemble (CE) model [38,54–59], which does not include discrete atomic states. Notably, the results from the CE model support the general concept that counter-rotating laser fields are more effective at exciting electrons, which leads to an ionization enhancement.

The use of bicircular fields is an ideal way to observe the dependence of photon spin on the strong-field ionization process, since it provides a very practical method for ensuring that the intensity of the field is maintained at the same value and that only the angular momentum of the incident photons is changed. The alternative approach would be to vary the polarization of a one-color field from linear to circular. Although this would certainly enable control of ionization via the photon spin, the peak electric field also changes as the polarization is changed from linear to circular, making it difficult to precisely compare ionization rates. We note that the temporal shape of the electric field changes in a bicircular field as the relative helicity is switched. However, this effect cannot be the cause of the ionization enhancement since the adiabatic ionization rates are the same for co- and counter-rotating fields at the same intensity ratio (see Appendix A).

II. EXPERIMENTAL METHODS

To study ionization yields in bicircular fields we mixed the fundamental of a Ti:sapphire laser (800 nm (ω), 40 fs, 5 kHz, KMLabs Wyvern HP) with its second harmonic [400 nm (2ω)] [Fig. 1(a)]. The fundamental beam was split into two arms of a Mach-Zehnder interferometer. In one arm the fundamental beam was frequency doubled in a 200-μm-thick beta barium borate crystal. The helicity of each laser pulse was controlled separately with wave plates ($\lambda/2$ and $\lambda/4$) in each arm while the intensity was controlled with a $\lambda/2$-wave-plate–thin-film-polarizer pair in each arm. Additionally, a one-to-one telescope was placed in the 800-nm arm to correct for chromatic aberration in the final focusing lens. The pulses were then focused with a 25-cm focal length lens onto a skimmed supersonic jet of helium, argon, or krypton gas. The positive ions were accelerated by a 2000-V static field in a 12-cm-long flight tube. The mass spectrum was recorded with a time-of-flight spectrometer consisting of microchannel plates, a collection anode, and a high-speed digitizer (Keysight Acqiris U1084A) used in the Peak$^{\mathrm{TDC}}$ operation mode. Each spectrum was averaged over 10^5 laser shots. The ionization yields are then recorded for the two possible relative helicities, and for four different $2\omega/\omega$ intensity ratios (I_B/I_R), as a function of the total intensity of the combined laser field. The ionization enhancement is calculated from the ionization ratio, $Y_{\mathrm{cr}}^{\mathrm{ion}}/Y_{\mathrm{co}}^{\mathrm{ion}}$, where $Y_{\mathrm{cr}}^{\mathrm{ion}}$ and $Y_{\mathrm{co}}^{\mathrm{ion}}$ are the ionization yields from counter- and co-rotating fields, respectively.

The intensity in each beam was independently calibrated using the same apparatus, but operating in a velocity-map-imaging [61] mode to detect photoelectrons (i.e., by changing the voltage and polarity of the electrodes). Photoelectron momentum distributions were then individually collected from both the fundamental and second-harmonic beams. These momentum distributions exhibit a peak at the ponderomotive energy (U_P) [62],

$$U_P = e^2 I/2c\epsilon_0 m_e \omega_0^2, \tag{1}$$

where I is the laser intensity, ω_0 is the angular frequency of the driving laser, e is the charge of the electron, c is the speed

of light, m_e is the mass of the electron, and ϵ_0 is the vacuum permittivity.

The phase delay between the two pulses was optimized for the best temporal overlap and remained constant during the data collection. However, drifts in the relative phase delay on the few-femtosecond time scale are unavoidable as the data was collected over many hours. Fortunately, since a change in the phase difference between the fundamental and second harmonic simply rotates the resulting electric field wave form [28,33,36], this experiment is not sensitive to slight phase drifts.

III. RESULTS AND DISCUSSION

A. Experimental results

The experimentally measured $Y_{\rm cr}^{\rm ion}/Y_{\rm co}^{\rm ion}$ ratios in helium, argon, and krypton for different I_B/I_R ratios (Fig. 2) exhibit the same general trend—counter-rotating fields induce significantly more ionization than their co-rotating counterparts over a range of intensities. Qualitatively, we can describe the ionization behavior under three intensity regimes: "low," "intermediate," and "high." Since the onset of tunnel ionization occurs at significantly different intensities for helium, argon, and krypton, we plot Fig. 2 in terms of the ponderomotive energy [U_P, Eq. (1)], which more readily demonstrates that the ionization enhancement occurs in the nonadiabatic regime. The onset of tunnel ionization is usually expressed in terms of U_P through the Keldysh parameter [63], $\gamma_{\rm K}$, which is given by $\gamma_{\rm K} = \omega_0/\Omega_{\rm tun} = \sqrt{I_P/2U_P}$, where ω_0 is the frequency of the laser, $\Omega_{\rm tun}$ is the tunneling frequency, and I_P is the ionization potential of the medium. The onset of tunnel ionization is roughly defined as $\gamma_{\rm k} > 1$.

Our experimental results show that at high values of U_P, where adiabatic tunnel ionization is the dominate ionization mechanism, the $Y_{\rm cr}^{\rm ion}/Y_{\rm co}^{\rm ion}$ ratio is near unity for all gases. In helium and krypton, when the U_P of the field is low and ionization occurs perturbatively (i.e., the multiphoton absorption of the high-energy 400-nm photons dominates the ionization process), the $Y_{\rm cr}^{\rm ion}/Y_{\rm co}^{\rm ion}$ ratio is again near unity. However, at intermediate U_P, where nonadiabatic ionization strongly contributes to the ionization yield [64–68] all three gases exhibit an enhancement in ionization for counter-rotating laser fields. Note that the low U_P behavior in argon differs from helium and krypton. Additionally, the shapes of the $Y_{\rm cr}^{\rm ion}/Y_{\rm co}^{\rm ion}$ ratios for helium, argon, and krypton are quite different, showing that two-color fields may offer a way of probing the electronic structure of atoms and molecules.

Although the ionization process discussed in this article is quite complex, since multiple photons from each of the pulses in the two-color (visible and NIR) field contribute to the ionization yield, we can propose a possible mechanism behind the observed difference in ionization rates for counter- and co-rotating bicircular laser fields in the nonadiabatic regime [Fig. 1(c)]. We assume that a significant fraction of ionization proceeds via a resonance-enhanced process, whereby several highly excited states of the ion (e.g., Rydberg states) are moved through a dynamically shifting and broadening multiphoton-accessible resonance [67–71]. In co-rotating fields, all photons have either $+1$ spin or -1 spin and thus only excited states with high angular momentum can be accessed. However, in counter-rotating laser fields, photons of both $+1$ and -1 spins are available and thus many more excited states (including those with low angular momenta) are available. The use of two-color fields provides an additional level of control over ionization, allowing for the contribution of spin-angular momentum to the ionization process to be isolated, as the peak electric field and integrated electric field remains the same for counter- and co-rotating fields.

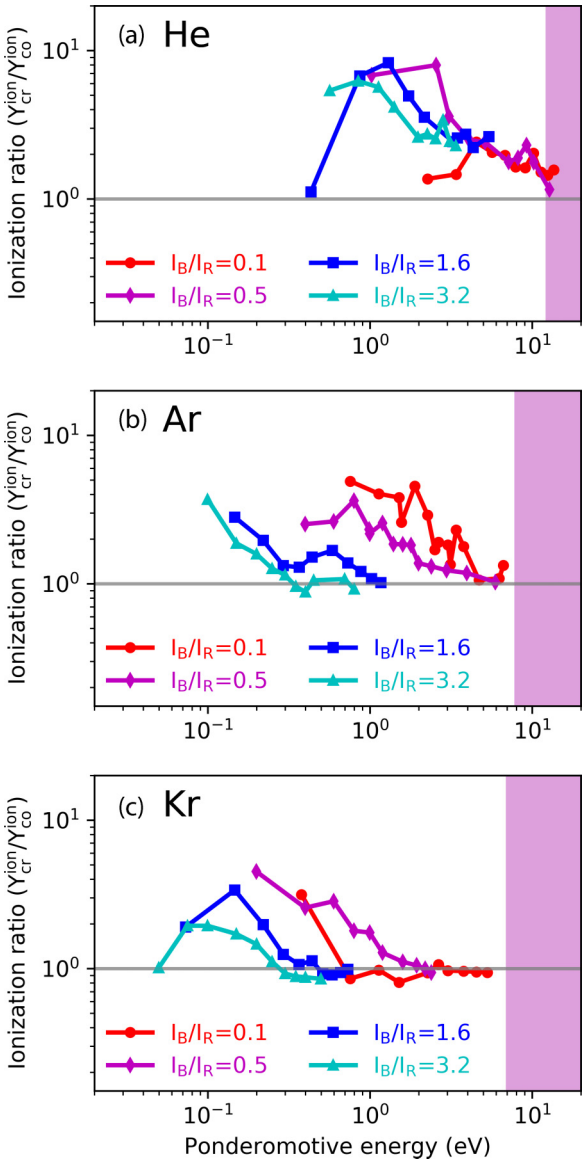

FIG. 2. Experimentally measured ionization yields in (a) helium, (b) argon, and (c) krypton. The measured ionization ratios, $Y_{\rm cr}^{\rm ion}/Y_{\rm co}^{\rm ion}$, where $Y_{\rm cr}^{\rm ion}$ and $Y_{\rm co}^{\rm ion}$ are the ionization yields from counter- and co-rotating fields, show that counter-rotating fields lead to enhanced ionization at intermediate values of the ponderomotive energy (U_P). The purple shaded region shows the onset of tunnel ionization (i.e., $U_P = I_P/2$).

B. TDSE simulations

To verify our experimental findings as well as to better understand the possible mechanism behind the ionization

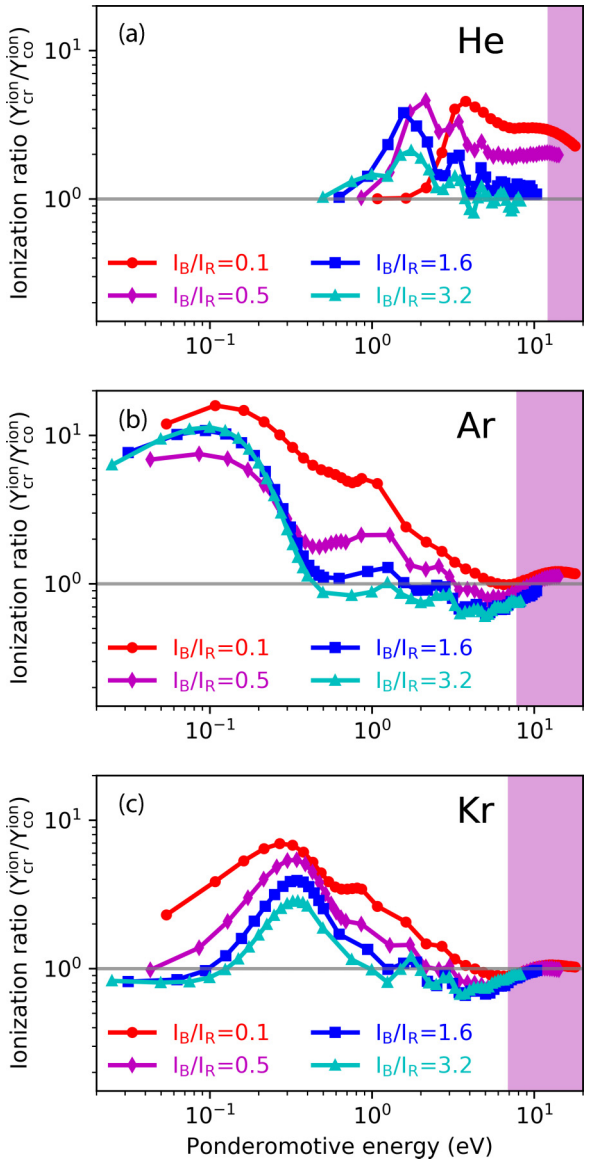

FIG. 3. TDSE simulations of the ionization yield in (a) helium, (b) argon, and (c) krypton. The simulated ionization ratios, $Y_{cr}^{ion}/Y_{co}^{ion}$, where Y_{cr}^{ion} and Y_{co}^{ion} are the ionization yields from counter- and co-rotating fields, show that counter-rotating fields lead to enhanced ionization at intermediate values of the ponderomotive energy (U_P). The purple shaded region shows the onset of tunnel ionization (i.e., $U_P = I_P/2$).

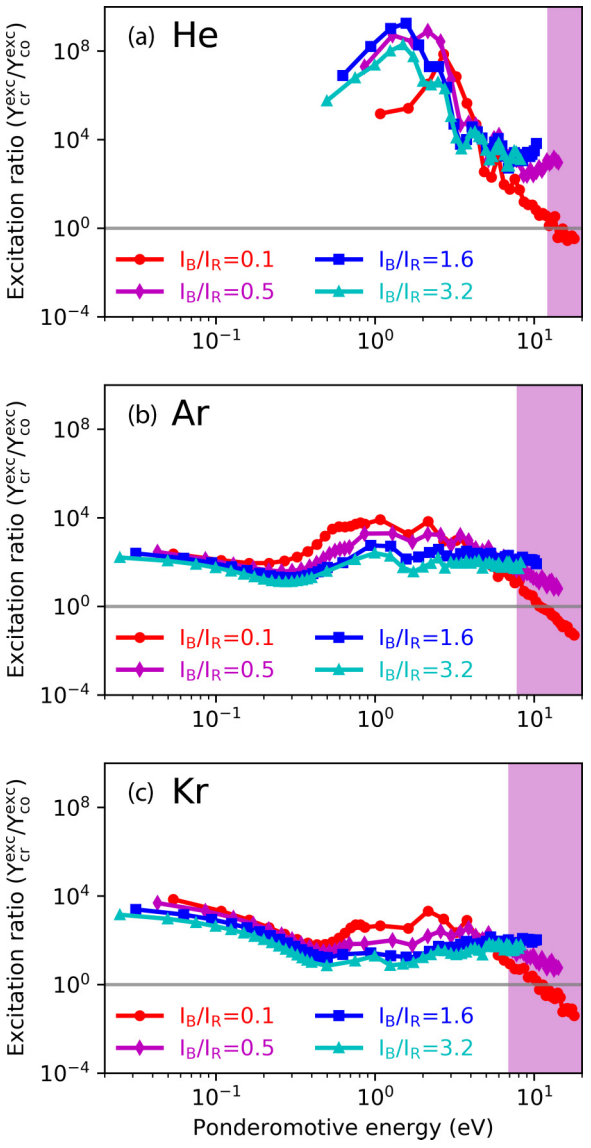

FIG. 4. TDSE simulations of the excitation probability in (a) helium, (b) argon, and (c) krypton. The simulated excitation ratio, $Y_{cr}^{exc}/Y_{co}^{exc}$, where Y_{cr}^{exc} and Y_{co}^{exc} are the probabilities that a counter- and co-rotating field will leave an atom in an excited state. The excitation ratio shows that counter-rotating fields more readily populate electrons to an excited state. The purple shaded region shows the onset of tunnel ionization (i.e., $U_P = I_P/2$).

enhancement, we employed TDSE simulations [52,53]. The TDSE simulations include perturbative ionization, resonantly enhanced multiphoton ionization (REMPI), and tunnel ionization. The simulations numerically solve the TDSE in the framework of the single-active electron model with a realistic model potential for the ground state of each gas and using a generalized pseudospectral method in the energy representation [53,72]. The ionization yields of helium, argon, and krypton obtained via the TDSE simulations (Fig. 3) support our experimental findings, showing the same trends between co- and counter-rotating fields in the three different ionization regimes.

Additionally, the TDSE simulations were used to calculate the excitation probability in these fields (Fig. 4), which is a measure of how many atoms are left in an excited state after the laser pulse has passed. The results show that for all three gases, counter-rotating fields more readily populate electrons to an excited state, supporting the explanation that the ionization enhancement results from an increased accessibility to spin-allowed transitions in counter-rotating fields.

To uncover a more general view of the underlying physics, we also used the TDSE simulations to calculate the $Y_{cr}^{ion}/Y_{co}^{ion}$ ratio for a larger number of I_B/I_R ratios [Fig. 5(a)]. In addition to reproducing the trends seen in Figs. 2 and 3, a number of "fingerlike" structures can be observed. These fingerlike

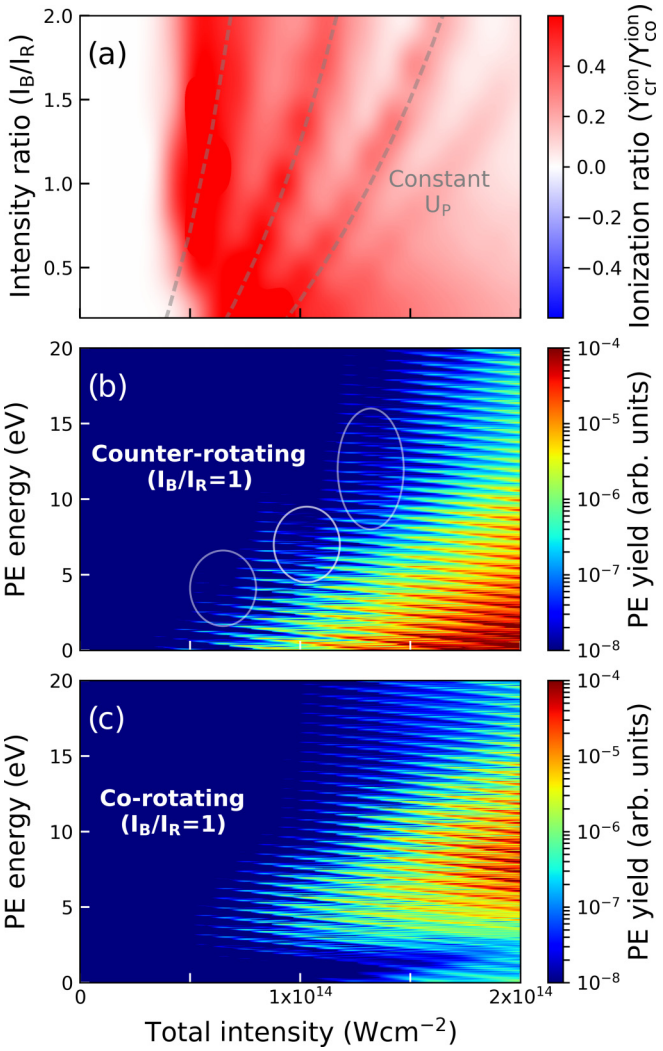

FIG. 5. TDSE simulations in helium. (a) The $Y_{cr}^{ion}/Y_{co}^{ion}$ ratio for a number of different I_B/I_R ratios shows "fingerlike" structures of similar $Y_{cr}^{ion}/Y_{co}^{ion}$ ratios that follow lines of constant ponderomotive energy, U_P (gray dashed lines). (b),(c) The photoelectron yield as a function of total intensity and photoelectron energy show that the fingerlike structures are due to channel-closing effects, which are only seen in the counter-rotating case. These channel closings [white ovals in (b)] result from excited states being dynamically broadened and shifted through a multiphoton resonance by the intense laser field. This effect is not seen in the co-rotating case because the angular momentum of the photons precludes resonance excitation to most states. Note that the presence of low-energy electrons for the counter-rotating field (b) and their absence in the co-rotating field (c) is due to both the shape of the fields as well as the increased role of electron-ion rescattering in counter-rotating fields [33,36].

structures follow lines of constant ponderomotive energy, U_P. These structures are a result of channel-closing effects [32,73–76], where excited states are shifted by a strong-field laser to an extent that they are no longer accessible via REMPI. The presence of channel-closing effects is indicative of REMPI, and these channel closings are observed more prominently in linear fields than circular fields [77], since circular fields can only access excited states with high angular momentum. A similar

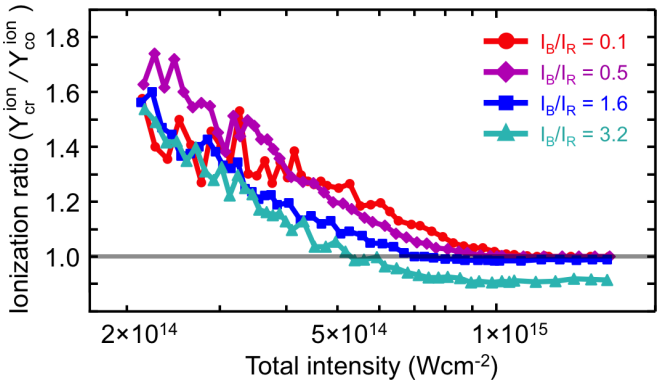

FIG. 6. Classical ensemble simulations of the ionization yields in helium. The ion yield ratio ($Y_{cr}^{ion}/Y_{co}^{ion}$) shows an ionization enhancement in counter-rotating fields, in qualitative agreement with the experimental results and TDSE simulations. An ion yield ratio of less than 1, which is observed for $I_B/I_R = 3.2$ at high total intensity, results from electrons that are driven back to the ion by counter-rotating fields and recombine to highly excited states (see Fig. 7). Each data point consists of an ensemble of 10^4 atoms to achieve a minimum of 500 ionization events.

REMPI ionization enhancement should be seen for co- and counter-rotating fields, since co-rotating fields can only access states with high angular momentum. At intensities where counter-rotating fields undergo a channel closing (and REMPI is the dominant ionization mechanism), the ionization rates between counter- and co-rotating fields should be equal, and at other intensities counter-rotating fields will lead to more ionization [Figs. 1(b) and 3]. It is worth noting that these channel-closing effects are difficult to detect in the experimental ion yield due to the spatially varying intensity of the laser within the focal volume.

To confirm that these fingerlike structures are indeed due to channel-closing effects, we calculated the photoelectron yield as a function of both the total intensity and the photoelectron energy [Figs. 5(b) and 5(c)]. For counter-rotating fields, as the intensity is increased there exist regions where the yield at a certain photoelectron energy sharply decreases. These jumps in the photoelectron yield, which are the signature of channel closings, are not present in the co-rotating data.

C. Classical ensemble simulations

We also study the ionization enhancement in helium using CE simulations [38,54–59]. For an expanded description of how the model was employed, see the Supplemental Material of Ref. [34]. Remarkably, even though these simulations are purely classical and do not include any quantum effects, an ionization enhancement is still observed in counter-rotating fields for a wide range of I_B/I_R ratios (Fig. 6), which is in qualitative agreement with the experimental and TDSE results.

To help explain the observed ionization enhancement in the CE model we examine the electron energy distribution after the laser pulse has ended at a total intensity of 5×10^{14} W cm^{-2} (Fig. 7). In classical analogy to the quantum picture, the CE simulations show that counter-rotating fields more readily excite electrons as compared to co-rotating fields (Fig. 7, blue shaded region). This generation of excited "classical Rydberg

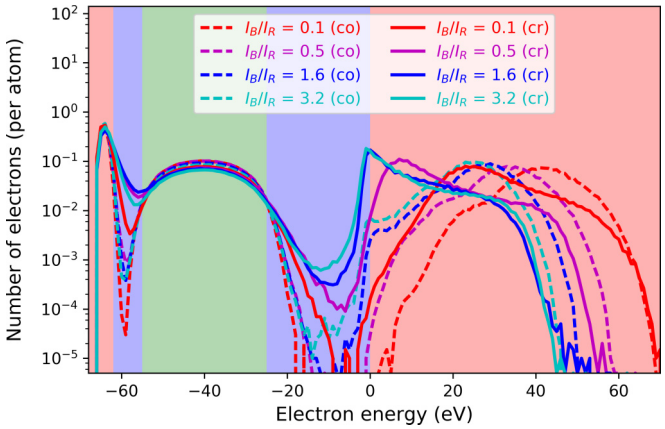

FIG. 7. The electron energy distribution at a total intensity of 5×10^{14} W cm^{-2} shows enhanced excitation in counter-rotating fields. The green shaded regions correspond to electrons in ground state He, where both the electrons are bound to the atom with energies centered at ∼40 eV, providing a total ground state energy of ∼79 eV. The red shaded regions correspond to He^+ electrons, where one electron is ionized (>0 eV) leaving the other electron tightly bound to the He^+ ion (<∼62 eV). The blue shaded regions represent excited state He, where one electron is excited to near 0 eV, leaving the other electron more tightly bound. The different shapes seen for the different I_B/I_R ratios for electron energies >0 eV is due to the different final drift energies of the fields [36]. The number of atoms in the ensemble is 2.5×10^5.

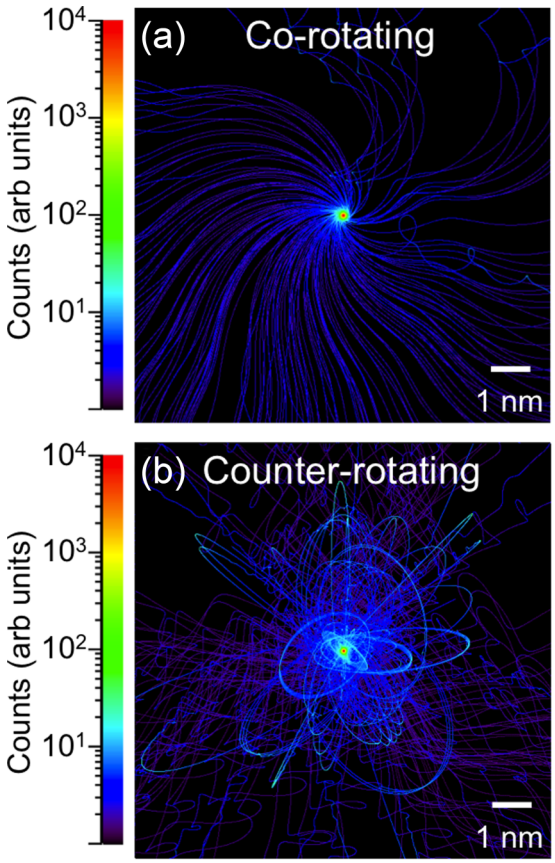

FIG. 8. Electron trajectories in the transverse plane show how counter-rotating fields can drive electrons into orbits similar to those of high-lying Rydberg states, whereas co-rotating fields do not. These electrons can be recaptured, leading to a decreased ionization enhancement for counter-rotating fields. The trajectories shown here are computed for $I_B/I_R = 3.2$, a total intensity of 5×10^{14} W cm^{-2}, and from -30 fs $< t <$ 120 fs from the peak of the 10-fs pulse. The number of atoms in the ensemble is 250.

states" is dramatically visualized with plots of ensembles of 250 electron trajectories, showing how counter-rotating fields allow electrons to become recaptured in large, highly excited orbits around the ion [Fig. 8(b)], whereas co-rotating fields do not [Fig. 8(a)]. This recapture of Rydberg electrons could explain the reduced ionization enhancement seen in both the TDSE and CE simulations for high I_B/I_R ratios, whereas in the experiment these electrons are ionized by the static field of the time-of-flight detector (see Appendix B). It is worth noting that the CE model is explicitly a strong-field model, and is not able to simulate the physics seen in the perturbative ionization regime at low intensities. This is the reason why the ionization enhancement never decreases as the total intensity is lowered in the CE simulations (Fig. 6).

Finally, to visualize the electron dynamics that lead to the observed ionization enhancement, we plot ensembles of electron trajectories just prior to the moment of ionization [Figs. 9(a) and 9(b)], showing that counter-rotating fields drive a greater number of electrons into large excursions that return to the ion prior to the final liberation of an electron, much like the orbits of Rydberg electrons with low angular momentum [78]. Additionally, counter-rotating fields also result in a population increase for electrons very close to the ion [Fig. 9(c)], corresponding to the more tightly bound counterpart to the highly excited electron.

The results from the CE simulations allow us to recognize that the observed ionization enhancement in counter-rotating fields is an indication of returning electron trajectories for *single* ionization, just as the observation of the familiar "knee" in nonsequential double ionization [79] for counter-rotating fields [34] is a signature of returning electron trajectories for *double* ionization. This similarity is notable as the strength of the electron-ion interaction is much different between the two processes. The measurement of this single ionization effect is made possible by the use of bicircular fields, where the shape of the fields is dramatically different for counter- and co-rotating fields, even though the peak field amplitude and average intensity are the same for both cases.

IV. CONCLUSION

In conclusion, we have shown that two-color counter-rotating fields lead to an enhancement in the ionization yield up to 700% compared with co-rotating fields, which occurs in the nonadiabatic ionization regime. This effect was observed both experimentally and theoretically in helium, argon, and krypton and for a number of different intensity ratios. We have also proposed a mechanism for this ionization enhancement in both the quantum-mechanical and classical pictures. In the quantum picture, the presence of both photon spin polarizations in counter-rotating fields allows access to a greater number of resonantly enhanced ionization pathways as compared to co-rotating fields, where the single spin-angular

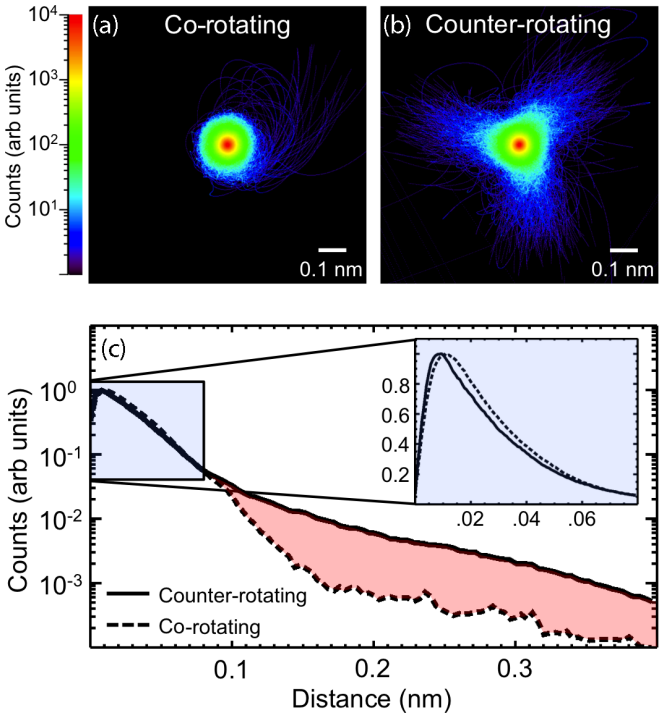

FIG. 9. (a),(b) Electron trajectories from an ensemble of 5000 atoms for $I_B/I_R = 1$ and an intensity of 4×10^{14} W cm^{-2}, shown from 2.67 fs before each atom is ionized, until the instant of ionization. (c) The histogram of the electron-ion separation for the trajectories shown in (a) and (b) shows that counter-rotating fields have higher concentrations of electrons at both longer (red shaded region) and shorter (inset) distances from the ion core compared to co-rotating fields.

momentum of the photons prevents excitation to excited states possessing low total angular momenta. In the classical picture, counter-rotating fields drive electrons in trajectories that enhance the absorption of energy from the laser field and enable ionization. These results show that bicircular fields can be used as a sensitive probe of the excited state manifold, which could be applied to more complicated molecules in the future. Moreover, the comparison of ionization in counter-rotating and co-rotating fields provides a straightforward and precise method of examining ionization in the nonadiabatic regime, and will be beneficial for all experiments looking at rescattering and recombination in these fields.

ACKNOWLEDGMENTS

H.K. and M.M. acknowledge support from the Department of Energy Office of Basic Energy Sciences (DOE BES) AMOS Award DE-FG02-99ER14982 and from the DOE BES X-Ray Scattering Program that provided the optical setup used in this work. J.E. and C.M. acknowledge support from National Science Foundation Graduate Research Fellowships (DGE-1144083). X.M.T. was supported by a Grant-in-Aid for Scientific Research [(C)JP16K05495] from the Japan Society for the Promotion of Science. TDSE calculations were performed using HA-PACS at Center for Computational Sciences, University of Tsukuba.

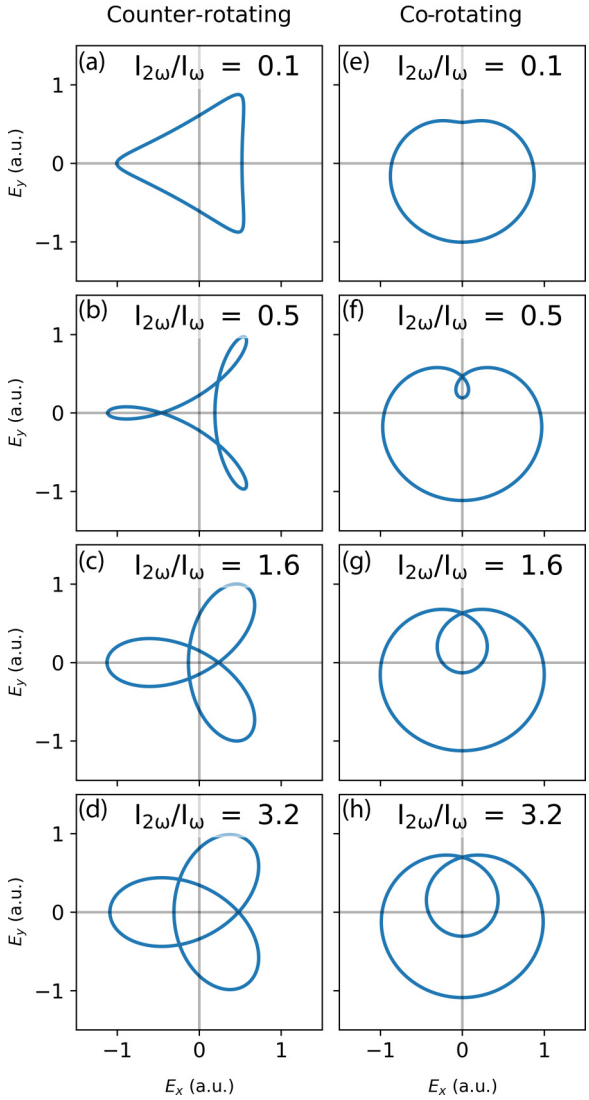

FIG. 10. The temporal shape of the electric fields for the experimental I_B/I_R ratios.

APPENDIX A: EFFECT OF THE TEMPORAL SHAPE OF THE ELECTRIC FIELD ON THE ADIABATIC TUNNEL-IONIZATION RATE

In a bicircular field as both the relative intensity and relative helicity is changed between the two beams, the resulting temporal shape of the electric field is changed as well (Fig. 10). To understand why this temporal shape difference cannot explain the observed ionization enhancement we calculated the Ammosov-Delone-Krainov (ADK) rates [80] for a bicircular field for each helicity at $I_B/I_R = 1$. The ADK rates give an estimation of ionization expected in the adiabatic tunnel-ionization regime. To numerically compute the average tunneling rate, the electric field of one cycle of an infinitely long bicircular field was discretized into 10^4 points. The ADK rate for each point was calculated as if it was the peak field of a one-color linearly polarized pulse [80–82]. The average [Fig. 11(a)] and peak [Fig. 11(b)] ADK rates are identical between co- and counter-rotating fields. This was additionally done for a number of other I_B/I_R ratios, and in all cases the

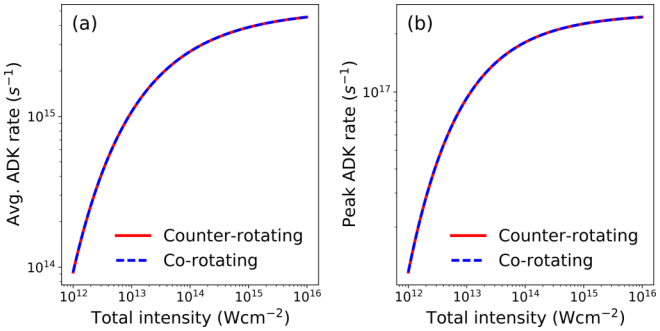

FIG. 11. The (a) average and (b) peak ADK rates show that in the adiabatic tunnel-ionization regime, there should be no difference in the ionization yields between co- and counter-rotating fields even though they have significantly different temporal shapes.

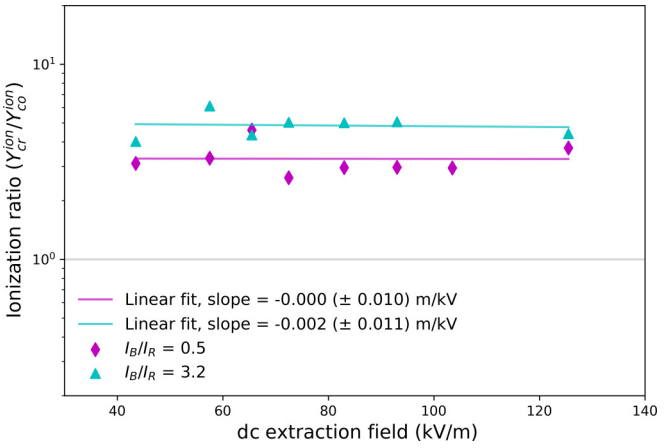

FIG. 12. The dc electric fields used to accelerate the electrons to the detector lead to ionization of electrons in high-lying Rydberg states. However, the dc fields are sufficiently high that we do not observe a change in the $Y_{cr}^{ion}/Y_{co}^{ion}$ ratio between co- and counter-rotating fields as the extraction field strength is varied.

yields for counter- and co-rotating fields were identical to each other for a given I_B/I_R ratio.

APPENDIX B: EFFECT OF EXTRACTION FIELD ON THE IONIZATION RATIOS

The laser excitation of bound electrons can lead to population of high-lying Rydberg states. These Rydberg states are only loosely bound to the atom, and thus can be ionized by the dc electric field used to accelerate the ions from the interaction region to the detector in the time-of-flight spectrometer [83,84]. Although in the experiment, the dc electric field was kept constant for all scans, we experimentally confirmed that the strength of the extraction field had no effect on the $Y_{cr}^{ion}/Y_{co}^{ion}$ ratio (Fig. 12). Here, we keep the extraction plate grounded and vary the voltage across the repeller plate from 1000 to 3000 V. The electric field at the interaction region was calculated using SIMION [85]. This was done for two laser conditions: (1) $I_B/I_R = 0.5$ at an intensity of 1.47×10^{14} W cm^{-2} and (2) $I_B/I_R = 3.2$ at an intensity of 1.85×10^{14} W cm^{-2}. We observed that these changes in the extraction field strength had no effect on the measured $Y_{cr}^{ion}/Y_{co}^{ion}$ ratio, as all field strengths were high enough to ionize electrons in high-lying Rydberg states.

[1] A. Mcpherson, G. Gibson, H. Jara, U. Johann, T. S. Luk, I. A. McIntyre, K. Boyer, and C. K. Rhodes, J. Opt. Soc. Am. B **4**, 595 (1987).

[2] M. Ferray, A. L'Huillier, X. F. Li, L. A. Lompre, G. Mainfray, and C. Manus, J. Phys. B: At., Mol. Opt. Phys. **21**, L31 (1988).

[3] M. Y. Kuchiev, Pis'ma Zh. Eksp. Teor. Fiz. **45**, 319 (1987) [JETP Lett. **45**, 404 (1987)].

[4] J. L. Krause, K. J. Schafer, and K. C. Kulander, Phys. Rev. Lett. **68**, 3535 (1992).

[5] M.-C. Chen, C. Mancuso, C. Hernández-García, F. Dollar, B. Galloway, D. Popmintchev, P.-C. Huang, B. Walker, L. Plaja, A. A. Jaroń-Becker, A. Becker, M. M. Murnane, H. C. Kapteyn, and T. Popmintchev, Proc. Natl. Acad. Sci. USA **111**, E2361 (2014).

[6] T. Popmintchev, M.-C. Chen, P. Arpin, M. M. Murnane, and H. C. Kapteyn, Nat. Photonics **4**, 822 (2010).

[7] A. Rundquist, C. G. Durfee, Z. Chang, C. Herne, S. Backus, M. M. Murnane, and H. C. Kapteyn, Science **280**, 1412 (1998).

[8] C. G. Durfee, A. R. Rundquist, S. Backus, C. Herne, M. M. Murnane, and H. C. Kapteyn, Phys. Rev. Lett. **83**, 2187 (1999).

[9] R. A. Bartels, A. Paul, H. Green, H. C. Kapteyn, M. M. Murnane, S. Backus, I. P. Christov, Y. Liu, D. Attwood, and C. Jacobsen, Science **297**, 376 (2002).

[10] T. Popmintchev, M.-C. Chen, D. Popmintchev, P. Arpin, S. Brown, S. Ališauskas, G. Andriukaitis, T. Balčiunas, O. D. Mücke, A. Pugzlys, A. Baltuška, B. Shim, S. E. Schrauth, A. Gaeta, C. Hernández-García, L. Plaja, A. Becker, A. Jaron-Becker, M. M. Murnane, and H. C. Kapteyn, Science **336**, 1287 (2012).

[11] R. Bartels, S. Backus, E. Zeek, L. Misoguti, G. Vdovin, I. P. Christov, M. M. Murnane, and H. C. Kapteyn, Nature (London) **406**, 164 (2000).

[12] S. Mathias, C. La-O-Vorakiat, P. Grychtol, P. Granitzka, E. Turgut, J. M. Shaw, R. Adam, H. T. Nembach, M. E. Siemens, S. Eich, C. M. Schneider, T. J. Silva, M. Aeschlimann, M. M. Murnane, and H. C. Kapteyn, Proc. Natl. Acad. Sci. USA **109**, 4792 (2012).

[13] E. Turgut, C. La-o-vorakiat, J. M. Shaw, P. Grychtol, H. T. Nembach, D. Rudolf, R. Adam, M. Aeschlimann, C. M. Schneider, T. J. Silva, M. M. Murnane, H. C. Kapteyn, and S. Mathias, Phys. Rev. Lett. **110**, 197201 (2013).

[14] S. Mathias, S. Eich, J. Urbancic, S. Michael, A. V. Carr, S. Emmerich, A. Stange, T. Popmintchev, T. Rohwer, M. Wiesenmayer *et al.*, Nat. Commun. **7**, 12902 (2016).

[15] Z. Tao, C. Chen, T. Szilvási, M. Keller, M. Mavrikakis, H. Kapteyn, and M. Murnane, Science **353**, 62 (2016).

[16] R. L. Sandberg, D. A. Raymondson, C. La-o-vorakiat, A. Paul, K. S. Raines, J. Miao, M. M. Murnane, H. C. Kapteyn, and W. F. Schlotter, Opt. Lett. **34**, 1618 (2009).

[17] J. Miao, T. Ishikawa, I. K. Robinson, and M. M. Murnane, Science **348**, 530 (2015).

[18] B. Zhang, D. F. Gardner, M. D. Seaberg, E. R. Shanblatt, H. C. Kapteyn, M. M. Murnane, and D. E. Adams, Ultramicroscopy **158**, 98 (2015).

[19] E. R. Shanblatt, C. L. Porter, D. F. Gardner, G. F. Mancini, R. M. Karl, M. D. Tanksalvala, C. S. Bevis, V. H. Vartanian, H. C. Kapteyn, D. E. Adams, and M. M. Murnane, Nano Lett. **16**, 5444 (2016).

[20] C. I. Blaga, J. Xu, A. D. DiChiara, E. Sistrunk, K. Zhang, P. Agostini, T. A. Miller, L. F. DiMauro, and C. D. Lin, Nature (London) **483**, 194 (2012).

[21] J. Xu, C. I. Blaga, K. Zhang, Y. H. Lai, C. D. Lin, T. A. Miller, P. Agostini, and L. F. DiMauro, Nat. Commun. **5**, 4635 (2014).

[22] M. G. Pullen, B. Wolter, A.-T. Le, M. Baudisch, M. Hemmer, A. Senftleben, C. D. Schröter, J. Ullrich, R. Moshammer, C. D. Lin, and J. Biegert, Nat. Commun. **6**, 7262 (2015).

[23] H. Eichmann, A. Egbert, S. Nolte, C. Momma, B. Wellegehausen, W. Becker, S. Long, and J. K. McIver, Phys. Rev. A **51**, R3414(R) (1995).

[24] S. Long, W. Becker, and J. K. McIver, Phys. Rev. A **52**, 2262 (1995).

[25] D. B. Milošević and W. Becker, Phys. Rev. A **62**, 011403(R) (2000).

[26] D. B. Milošević, W. Becker, and R. Kopold, Phys. Rev. A **61**, 063403 (2000).

[27] A. Fleischer, O. Kfir, T. Diskin, P. Sidorenko, and O. Cohen, Nat. Photonics **8**, 543 (2014).

[28] O. Kfir, P. Grychtol, E. Turgut, R. Knut, D. Zusin, D. Popmintchev, T. Popmintchev, H. Nembach, J. M. Shaw, A. Fleischer, H. Kapteyn, M. Murnane, and O. Cohen, Nat. Photonics **9**, 99 (2015).

[29] K. M. Dorney, J. L. Ellis, C. Hernández-García, D. D. Hickstein, C. A. Mancuso, N. Brooks, T. Fan, G. Fan, D. Zusin, C. Gentry, P. Grychtol, H. C. Kapteyn, and M. M. Murnane, Phys. Rev. Lett. (to be published).

[30] T. Fan, P. Grychtol, R. Knut, C. Hernández-García, D. D. Hickstein, D. Zusin, C. Gentry, F. J. Dollar, C. A. Mancuso, C. W. Hogle *et al.*, Proc. Natl. Acad. Sci. USA **112**, 14206 (2015).

[31] A. Kramo, E. Hasović, D. B. Milošević, and W. Becker, Laser Phys. Lett. **4**, 279 (2007).

[32] E. Hasović, A. Kramo, and D. B. Milošević, Eur. Phys. J.: Spec. Top. **160**, 205 (2008).

[33] C. A. Mancuso, D. D. Hickstein, P. Grychtol, R. Knut, O. Kfir, X.-M. Tong, F. Dollar, D. Zusin, M. Gopalakrishnan, C. Gentry, E. Turgut, J. L. Ellis, M.-C. Chen, A. Fleischer, O. Cohen, H. C. Kapteyn, and M. M. Murnane, Phys. Rev. A **91**, 031402(R) (2015).

[34] C. A. Mancuso, K. M. Dorney, D. D. Hickstein, J. L. Chaloupka, J. L. Ellis, F. J. Dollar, R. Knut, P. Grychtol, D. Zusin, C. Gentry, M. Gopalakrishnan, H. C. Kapteyn, and M. M. Murnane, Phys. Rev. Lett. **117**, 133201 (2016).

[35] S. Eckart, M. Richter, M. Kunitski, A. Hartung, J. Rist, K. Henrichs, N. Schlott, H. Kang, T. Bauer, H. Sann, L. P. H. Schmidt, M. Schöffler, T. Jahnke, and R. Dörner, Phys. Rev. Lett. **117**, 133202 (2016).

[36] C. A. Mancuso, D. D. Hickstein, K. M. Dorney, J. L. Ellis, E. Hasović, R. Knut, P. Grychtol, C. Gentry, M. Gopalakrishnan, D. Zusin, F. J. Dollar, X.-M. Tong, D. B. Milošević, W. Becker, H. C. Kapteyn, and M. M. Murnane, Phys. Rev. A **93**, 053406 (2016).

[37] D. B. Milošević, Phys. Rev. A **93**, 051402(R) (2016).

[38] J. L. Chaloupka and D. D. Hickstein, Phys. Rev. Lett. **116**, 143005 (2016).

[39] E. Hasović, W. Becker, and D. B. Milošević, Opt. Express **24**, 6413 (2016).

[40] E. Hasović, S. Odžak, W. Becker, and D. B. Milošević, in *Molecular Physics* (Taylor & Francis, London, 2016), pp. 1–8.

[41] A. D. Bandrauk, F. Mauger, and K.-J. Yuan, J. Phys. B: At., Mol. Opt. Phys. **49**, 23LT01 (2016).

[42] T. Herath, L. Yan, S. K. Lee, and W. Li, Phys. Rev. Lett. **109**, 043004 (2012).

[43] I. Barth and O. Smirnova, Phys. Rev. A **84**, 063415 (2011).

[44] J. H. Bauer, F. Mota-Furtado, P. F. O'Mahony, B. Piraux, and K. Warda, Phys. Rev. A **90**, 063402 (2014).

[45] Y. Li, P. Lan, H. Xie, M. He, X. Zhu, Q. Zhang, and P. Lu, Opt. Express **23**, 28801 (2015).

[46] X. Zhu, P. Lan, K. Liu, Y. Li, X. Liu, Q. Zhang, I. Barth, and P. Lu, Opt. Express **24**, 4196 (2016).

[47] R. Taïeb, V. Véniard, A. Maquet, N. L. Manakov, and S. I. Marmo, Phys. Rev. A **62**, 013402 (2000).

[48] A. K. Kazansky, A. V. Grigorieva, and N. M. Kabachnik, Phys. Rev. A **85**, 053409 (2012).

[49] T. Mazza, M. Ilchen, A. J. Rafipoor, C. Callegari, P. Finetti, O. Plekan, K. C. Prince, R. Richter, M. B. Danailov, A. Demidovich *et al.*, Nat. Commun. **5**, 250 (2014).

[50] N. Douguet, A. N. Grum-Grzhimailo, E. V. Gryzlova, E. I. Staroselskaya, J. Venzke, and K. Bartschat, Phys. Rev. A **93**, 033402 (2016).

[51] M. Ilchen, N. Douguet, T. Mazza, A. J. Rafipoor, C. Callegari, P. Finetti, O. Plekan, K. C. Prince, A. Demidovich, C. Grazioli *et al.*, Phys. Rev. Lett. **118**, 013002 (2017).

[52] X. M. Tong, K. Hino, and N. Toshima, Phys. Rev. A **74**, 031405(R) (2006).

[53] X.-M. Tong and S.-I. Chu, Phys. Rev. A **58**, R2656(R) (1998).

[54] R. Panfili, S. L. Haan, and J. H. Eberly, Phys. Rev. Lett. **89**, 113001 (2002).

[55] P. J. Ho, R. Panfili, S. L. Haan, and J. H. Eberly, Phys. Rev. Lett. **94**, 093002 (2005).

[56] S. L. Haan, L. Breen, A. Karim, and J. H. Eberly, Phys. Rev. Lett. **97**, 103008 (2006).

[57] S. L. Haan, J. S. Van Dyke, and Z. S. Smith, Phys. Rev. Lett. **101**, 113001 (2008).

[58] J. Javanainen, J. H. Eberly, and Q. Su, Phys. Rev. A **38**, 3430 (1988).

[59] D. Bauer, Phys. Rev. A **56**, 3028 (1997).

[60] N. Shivaram, H. Timmers, X.-M. Tong, and A. Sandhu, Phys. Rev. Lett. **108**, 193002 (2012).

[61] A. T. J. B. Eppink and D. H. Parker, Rev. Sci. Instrum. **68**, 3477 (1997).

[62] W. Becker, F. Grasbon, R. Kopold, D. B. Milošević, G. G. Paulus, and H. Walther, Adv. At., Mol., Opt. Phys. **48**, 35 (2002).

[63] L. V. Keldysh, J. Exptl. Theoret. Phys. USSR **47**, 1945 (1964) [Sov. Phys. JETP **20**, 1307 (1965)].

[64] V. Tagliamonti, P. Sándor, A. Zhao, T. Rozgonyi, P. Marquetand, and T. Weinacht, Phys. Rev. A **93**, 051401(R) (2016).

[65] M. Li, J.-W. Geng, M. Han, M.-M. Liu, L.-Y. Peng, Q. Gong, and Y. Liu, Phys. Rev. A **93**, 013402 (2016).
[66] G. L. Yudin and M. Y. Ivanov, Phys. Rev. A **64**, 013409 (2001).
[67] J. C. Miller, R. N. Compton, M. G. Payne, and W. W. Garrett, Phys. Rev. Lett. **45**, 114 (1980).
[68] R. N. Compton, J. C. Miller, A. E. Carter, and P. Kruit, Chem. Phys. Lett. **71**, 87 (1980).
[69] N. B. Delone and V. P. Krainov, Phys. Usp. **42**, 669 (1999).
[70] P. Ranitovic, X. M. Tong, C. W. Hogle, X. Zhou, Y. Liu, N. Toshima, M. M. Murnane, and H. C. Kapteyn, Phys. Rev. Lett. **106**, 193008 (2011).
[71] S. I. Chu, in *Review of Fundamental Processes and Applications of Atoms and Ions*, edited by C. D. Lin (World Scientific Publishing Co., Singapore, 1993), pp. 403–440.
[72] X.-M. Tong and S.-I. Chu, Chem. Phys. **217**, 119 (1997).
[73] G. G. Paulus, F. Grasbon, H. Walther, R. Kopold, and W. Becker, Phys. Rev. A **64**, 021401 (2001).
[74] R. Kopold, W. Becker, M. Kleber, and G. G. Paulus, J. Phys. B: At., Mol. Opt. Phys. **35**, 217 (2002).
[75] Q. Li, X.-M. Tong, T. Morishita, H. Wei, and C. D. Lin, Phys. Rev. A **89**, 023421 (2014).
[76] E. Hasović, M. Busuladžić, A. Gazibegović-Busuladžić, D. B. Milošević, and W. Becker, Laser Phys. **17**, 376 (2007).
[77] P. H. Bucksbaum, L. D. Van Woerkom, R. R. Freeman, and D. W. Schumacher, Phys. Rev. A **41**, 4119 (1990).
[78] C. E. Theodosiou, Phys. Rev. A **28**, 3098 (1983).
[79] B. Walker, B. Sheehy, L. F. DiMauro, P. Agostini, K. J. Schafer, and K. C. Kulander, Phys. Rev. Lett. **73**, 1227 (1994).
[80] M. V. Ammosov, N. B. Delone, and V. P. Krainov, Zh. Eksp. Teor. Fiz. **91**, 2008 (1986) [Sov. Phys. JETP **64**, 1191 (1986)].
[81] N. B. Delone and V. P. Krainov, J. Opt. Soc. Am. B **8**, 1207 (1991).
[82] B. M. Penetrante and J. N. Bardsley, Phys. Rev. A **43**, 3100 (1991).
[83] Y. Ni, S. Zamith, F. Lépine, T. Martchenko, M. Kling, O. Ghafur, H. G. Muller, G. Berden, F. Robicheaux, and M. J. J. Vrakking, Phys. Rev. A **78**, 013413 (2008).
[84] C. T. L. Smeenk, L. Arissian, B. Zhou, A. Mysyrowicz, D. M. Villeneuve, A. Staudte, and P. B. Corkum, Phys. Rev. Lett. **106**, 193002 (2011).
[85] D. A. Dahl, Int. J. Mass Spectrom. **200**, 3 (2000).